



Extracellular vesicle-dependent effect of RNA-binding protein IGF2BP1 on melanoma metastasis

Archita Ghoshal¹ · Lucas C. Rodrigues¹ · Chethana P. Gowda¹ · Irina A. Elcheva¹ · Zhenqiu Liu¹ · Thomas Abraham² · Vladimir S. Spiegelman¹

Received: 26 September 2018 / Revised: 15 March 2019 / Accepted: 15 March 2019 / Published online: 1 April 2019
© Springer Nature Limited 2019

Abstract

Insulin-like growth factor 2 mRNA-binding protein 1 (IGF2BP1) is a multifunctional RNA-binding protein with an oncofetal pattern of expression shown to be implicated in the development of a variety of malignancies. In this study, we explored the role and mechanisms of IGF2BP1 in melanoma development and progression. In two different in vivo models, we showed that although genetic deletion or shRNA-mediated suppression of IGF2BP1 did not affect primary tumor formation, it drastically suppressed lung metastasis. Here we demonstrated that extracellular vesicles (EVs) secreted by melanoma cells mediate the effects of IGF2BP1 on metastasis: EVs from the IGF2BP1 knockdown melanoma cells failed to promote metastasis, whereas EVs isolated from IGF2BP1-overexpressed melanoma cells further accelerated EV-induced metastasis. Moreover, the EVs from IGF2BP1 knockdown melanoma cells inhibited fibronectin deposition and accumulation of CD45⁺ cells in the lungs compared with control EVs, thus blocking the pre-metastatic niche formation potential of EVs. IGF2BP1 knockdown did not affect size, number, or protein/RNA concentration of secreted EVs or their uptake by recipient cells in vitro or in vivo. However, RNA-sequencing and proteomics analysis of the EVs revealed differential expression in a number of mRNA, proteins, and miRNAs. This suggested that IGF2BP1 is intimately involved in the regulation of the cargo of EVs, thereby affecting the pro-metastatic function of melanoma-derived EVs. To the best of our knowledge, this is the first study that demonstrates the role of RNA-binding protein IGF2BP1 in EV-mediated promotion of melanoma metastasis and may provide novel avenues for the development of metastatic inhibitors.

Introduction

Insulin-like growth factor 2 mRNA-binding protein 1 (IGF2BP1), also commonly known as IMP1 or coding region determinant-binding protein (CRD-BP), is a

multifaceted RNA-binding, oncofetal protein that plays a role in a multitude of processes. Although it is expressed during embryogenesis in fetal and neonatal tissues in copious amounts, IGF2BP1 is undetectable in most adult tissues. However, it is aberrantly overexpressed in a number of tumor types and de novo synthesis of IGF2BP1 has been reported in a number of human cancers. Its elevated expression has been found to directly correlate with poor prognosis in most cancer types [1, 2]. Several reports have demonstrated that IGF2BP1 stabilizes the mRNA of proliferative or tumor-promoting genes, including *c-myc*, *βTrCP1*, *GLI1*, *MITF*, and *MDR1* [3–9]. It is also involved in posttranscriptional regulation of transcripts encoding proteins for cell adhesion, invasion, cytoplasmic spreading, and matrix remodeling (reviewed in ref. [10]).

Melanoma is an extremely metastatic form of skin cancer, which has been on a steady rise for the past three decades. Although it accounts for only 1% of all skin cancers, it causes a majority of deaths from skin cancer due to its aggressive nature. We have previously demonstrated

These authors contributed equally: Archita Ghoshal, Lucas C. Rodrigues

Supplementary information The online version of this article (<https://doi.org/10.1038/s41388-019-0797-3>) contains Supplementary Material, which is available to authorized users.

✉ Vladimir S. Spiegelman
vspiegelman@pennstatehealth.psu.edu

¹ Division of Pediatric Hematology/Oncology, Department of Pediatrics, Pennsylvania State University College of Medicine, Hershey, PA 17033, USA

² Department of Neural and Behavioral Science, Pennsylvania State University College of Medicine, Hershey, PA 17033, USA

that IGF2BP1 is upregulated in melanomas and have investigated the role of IGF2BP1 in melanoma in cell culture systems [11, 12]. Knockdown of IGF2BP1 has been shown to sensitize certain types of melanoma either to BRAF/BRAF-MEK inhibitors [13] or to chemotherapeutic agents [12]. However, the contribution of this RNA-binding protein to the metastatic spread of melanoma has not been explored *in vivo*.

Recent research has unveiled novel components of the secretome, which have been shown to be crucial to tumor progression [14–17]. These secreted factors, extracellular vesicles (EVs) and their subcategory—exosomes [18], transport functional proteins, nucleic acids, and lipids to recipient cells—thereby reprogramming them. Recent studies in different tumor models have also emphasized the key contribution of exosomes in driving pre-metastatic niche initiation, to prepare distant sites for the homing of cancer cells via the “education” of bone marrow-derived cells [14, 19, 20].

In this study, we aimed to delineate the role of IGF2BP1 in metastasis of melanoma, utilizing two different mouse models. We showed that suppression of IGF2BP1 drastically inhibits melanoma metastasis *in vivo*. Specifically, we demonstrated that EVs mediate the effect of IGF2BP1 on metastasis by affecting the formation of pre-metastatic niche. We found that inhibiting IGF2BP1 altered the cargo of the EVs, which potentially regulated a plethora of signaling networks, culminating in the inhibition of metastasis.

Results

Genetic deletion of IGF2BP1 suppresses melanoma metastasis

To determine the contribution of IGF2BP1 to tumor progression, we used a well-established BRAF/PTEN mouse model of melanoma [21] in combination with IGF2BP1^{loxP/loxP} mice that we have developed previously [22]. Herein, we observed a marked difference in lymph node metastasis between IGF2BP1-WT (Tyr::CreER^{T2} PTEN^{loxP/loxP} BraF^{F-V6000/+}) control and IGF2BP1 knockout (Tyr::CreER^{T2} PTEN^{loxP/loxP} BraF^{F-V6000/+} IGF2BP1^{loxP/loxP}) groups of mice when topical administration of tamoxifen was used to induce BRAF^{V600E} expression along with PTEN (phosphatase and tensin homolog) and IGF2BP1 deletion in melanocytes. The percentage of mice bearing metastatic lesions in the lymph node was significantly higher in the control group than in the knockout group (Fig. 1a). Although metastasis to lungs is not common in the PTEN^{loxP/loxP} BraF^{F-V6000/+} mouse model [21], 20% of the mice in the control group of our study were found to develop metastatic lung lesions. This number was notably higher compared with the IGF2BP1 knockout group in which

none of the mice displayed lung metastasis (Fig. 1b). Surprisingly, there was no significant difference in the primary tumor formation between the control and IGF2BP1 knockout groups. Even though tumor appearance was slightly delayed in the IGF2BP1 knockout group compared with the control group, there was no significant difference in their survival or tumor volume at the conclusion of the experiment (Supplementary Fig. S1A–C). Similarly, no significant differences in primary tumor development were observed when tamoxifen was administered intraperitoneally in the same mouse model (Supplementary Fig. S1D–E).

Knocking down IGF2BP1 reduces metastasis in syngeneic metastasis model

To validate the results obtained in our PTEN^{loxP/loxP} BraF^{F-V6000/+} mouse model in a different mouse model, we used a syngeneic mouse model to elucidate the role of IGF2BP1 in metastasis. A marginal difference was observed in the primary tumor volume between the two groups of mice that were injected with control (uninduced pInducer24 shIGF2BP1 construct) and doxycycline-induced IGF2BP1 knockdown SW1 cells pInducer24 (Fig. 1c). Also, in keeping with the observations from our previous model, we found a substantial reduction in the number of metastatic lesions in the lungs of the mice that received IGF2BP1 knockdown SW1 pInducer24 cells compared with the control group (Fig. 1d, e). In fact, the mice injected with control cells did not exhibit any metastatic lesion in the lungs as observed after sectioning and staining (Fig. 1f). These experiments were duplicated with SW1 cells having the M1 shIGF2BP1 construct in lieu of the pInducer24 construct and similar results were obtained as above (Supplementary Fig. S2). These data suggest that even though suppression of IGF2BP1 hardly affected the growth and development of the primary tumors, it drastically inhibited melanoma metastasis. A control cohort of mice was used to confirm that doxycycline-containing food did not affect lung metastasis (Supplementary Fig. S3).

To understand the contribution of IGF2BP1 to melanoma metastasis at the stage where circulating tumor cells exit the blood stream and form colonies in the lungs, we have intravenously (i.v.) injected SW1 cells into tail vein of the C3H mice (Supplementary Fig. S4). Interestingly, inhibition of IGF2BP1 did not affect the ability of melanoma cells to metastasize, suggesting that IGF2BP1 plays a minimal (if any) role in their extravasation and lung colonization.

Overexpression of IGF2BP1 correlates with poor clinical outcomes in melanoma patients

Given our results on the role of IGF2BP1 in melanoma metastasis in mouse models, we sought to elucidate whether

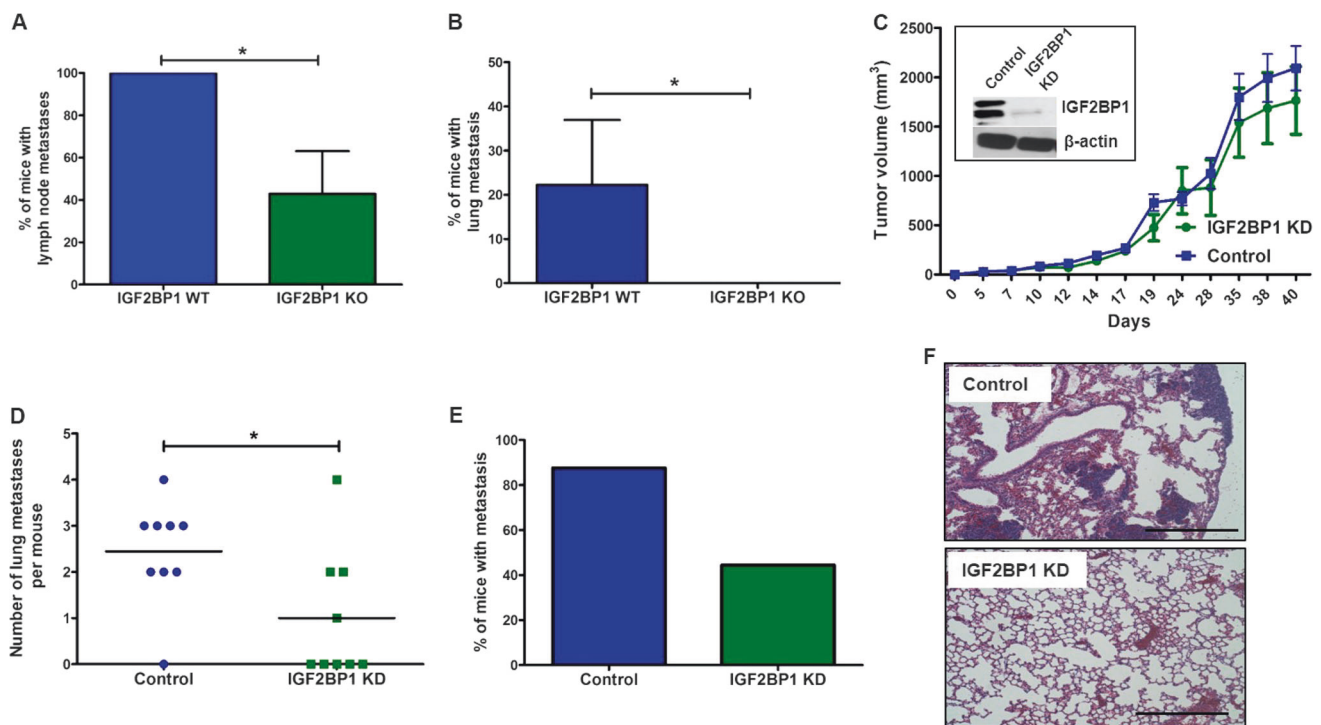


Fig. 1 Metastasis study in two different mouse models. **a, b** Localized tamoxifen induction (4-HT 5 mM) in IGF2BP1-WT (Tyr::CreERT2 PTEN^{loxP/loxP} Braf F-V6000/+) and IGF2BP1 knockout (Tyr::CreERT2 PTEN^{loxP/loxP} Braf F-V6000/+ IGF2BP1^{loxP/loxP}) mice. **a** Percentage of mice with lymph node metastasis ($p = 0.0263$, Student's t -test). **b** Percentage of mice with lung metastasis. IGF2BP1 WT mice had more lung metastasis compared to KO mice ($p = 0.0283$, Student's t -test). **c–f** The role of IGF2BP1 was evaluated in vivo using a syngeneic metastasis model. The potential of lung metastasis of SW1 pInducer24 melanoma cell lines—untreated (control) and

treated with doxycycline (to induce shRNA-mediated knockdown of IGF2BP1)—was evaluated in C3H mice. **c** Primary tumor volume of mice belonging to control ($n = 8$) and knockdown (KD) groups ($n = 10$). Inset: Western blotting showing knockdown of IGF2BP1 in mouse tissues. **d** Number of lung metastasis developed in each mouse from the control and knockdown groups ($p = 0.0293$, t -test). **e** Percentage of lung metastasis in control mice compared with IGF2BP1 knockdown group. **f** Microscopic evaluation of lungs of control and IGF2BP1 knockdown mice stained with H&E. Scale bar is 500 μm

the levels of IGF2BP1 expression are associated with clinical outcomes in melanoma patients. Statistical analysis of patient data available in The Cancer Genome Atlas showed that IGF2BP1 levels are strongly associated with patient survival (Supplementary Fig. S5). Patients without IGF2BP1 overexpression were found to have a threefold higher median survival than patients with an overexpression of the gene. Disease-free survival was also found to be more than threefold higher in patients without IGF2BP1 overexpression as opposed to patients with IGF2BP1 overexpression. As patient mortality is primarily determined by the extent of melanoma metastasis, our data revealing the role of IGF2BP1 in metastasis seemed to be in accordance with these statistics.

Inhibition of IGF2BP1 does not affect intrinsic pro-metastatic properties of mouse melanoma cells

In order to understand the mechanisms responsible for IGF2BP1 effects on metastasis, we first assessed whether it regulates the pro-metastatic intrinsic properties of

SW1 cells. With this aim, we analyzed changes in migration and invasion potential of SW1 cells after knocking down IGF2BP1. The cell migration assay did not reveal a significant difference between the control and IGF2BP1 knockdown cells (Supplementary Fig. S6A). Although IGF2BP1 knockdown cells showed lesser invasive properties than the control cells in the invasion assay (Supplementary Fig. S6B), the difference was not significant.

Inhibition of IGF2BP1 does not significantly affect secretion of cytokines and chemokines by melanoma cells

As IGF2BP1 had a dramatic effect on metastasis without altering the intrinsic pro-metastatic properties of the melanoma cells, we hypothesized that it can affect factors secreted by melanoma cells that influence metastasis through interaction with tumor microenvironment or distant sites. Intriguingly, the top pathways that were identified in a gene enrichment analysis of RNA-sequencing (RNA-seq) data (heatmap showed in Supplementary Fig. S7) were

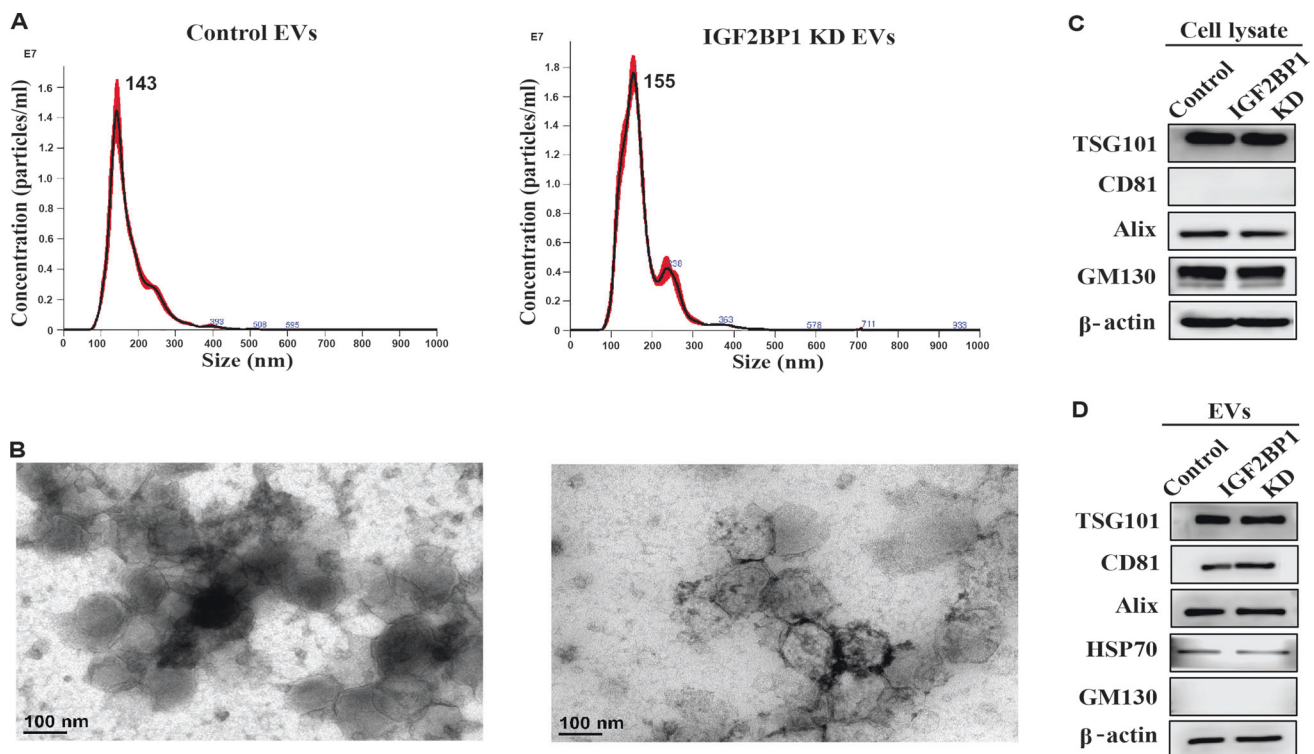


Fig. 2 Analysis of EVs isolated from control and IGF2BP1 knock-down SW1 cells using sucrose cushion method. **a** Nanoparticle-tracking analysis (NTA). **b** Transmission electron microscopy (TEM)

imaging. **c, d** Western blotting for starting cellular material and EVs to probe exosomal and golgi markers

cytokine and chemokine networks (Supplementary Fig. S7), which led us to postulate that IGF2BP1 could affect these secretory growth factors to alter the tumor microenvironment *in vivo*. However, an extensive cytokine profile panel of 32 different cytokines (Supplementary Fig. S8) from the *in vitro* culture media of control and IGF2BP1 knockdown SW1 cells revealed that there was no significant difference between the groups, in spite of the difference found at the mRNA level. This ruled out the possibility of a cytokine-mediated effect of IGF2BP1 on melanoma metastasis.

Characterization of EVs isolated from the media of IGF2BP1 knockdown melanoma cells

Building on the above rationale, we explored the possibility that EVs, which are cell-derived vesicles of endocytic origin carrying abundant nucleic acids and proteins, might mediate the role of IGF2BP1 in metastasis. EVs in the size range of 30–150 nm are typically called exosomes. As accumulating evidence suggests that exosomes contribute to metastasis primarily via the formation of pre-metastatic niche [14, 20], we investigated the role of the EVs in our study. We isolated EVs from control and IGF2BP1 knockdown SW1 cells using two different methods of purification as elaborated in the Methods section. The isolated EVs were characterized with Nanosight nanoparticle-tracking analysis

(NTA), transmission electron microscopy (TEM), and western blottings. NTA and TEM analyses revealed that the isolated particles ranged from 100 to 150 nm in size, which is within the acceptable size range for exosomes. Figure 2a, b, demonstrating the NTA and TEM analyses, respectively, illustrate that the EVs isolated with the sucrose cushion method were highly homogenous in size. Supplementary Fig. S9A and B show the same for the EVs isolated with the regular ultracentrifugation method. However, there was no difference in size between the EVs isolated from control and IGF2BP1 knockdown SW1 cells in either case. NTA data also illustrated that there was no significant difference in the concentration of particles (calculation not shown). Moreover, there was no difference in the concentration of protein between the control and IGF2BP1 knockdown samples (data not shown). Western blottings, probing exosomal marker proteins CD81, HSP70, Alix, and TSG101, validated the presence of EVs (Fig. 2 and Supplementary Fig. S9C). Interestingly, probing the expression of IGF2BP1 in the EVs by western blotting revealed a faint band for IGF2BP1 in the EVs derived from control cells, which was absent in the EVs from IGF2BP1 knockdown cells (Supplementary Fig. S9C). Starting cellular material was also analyzed in the western blottings to show the enrichment of exosomal markers in the EVs in comparison with the cell lysates (Fig. 2). Golgi marker GM130 was used as a

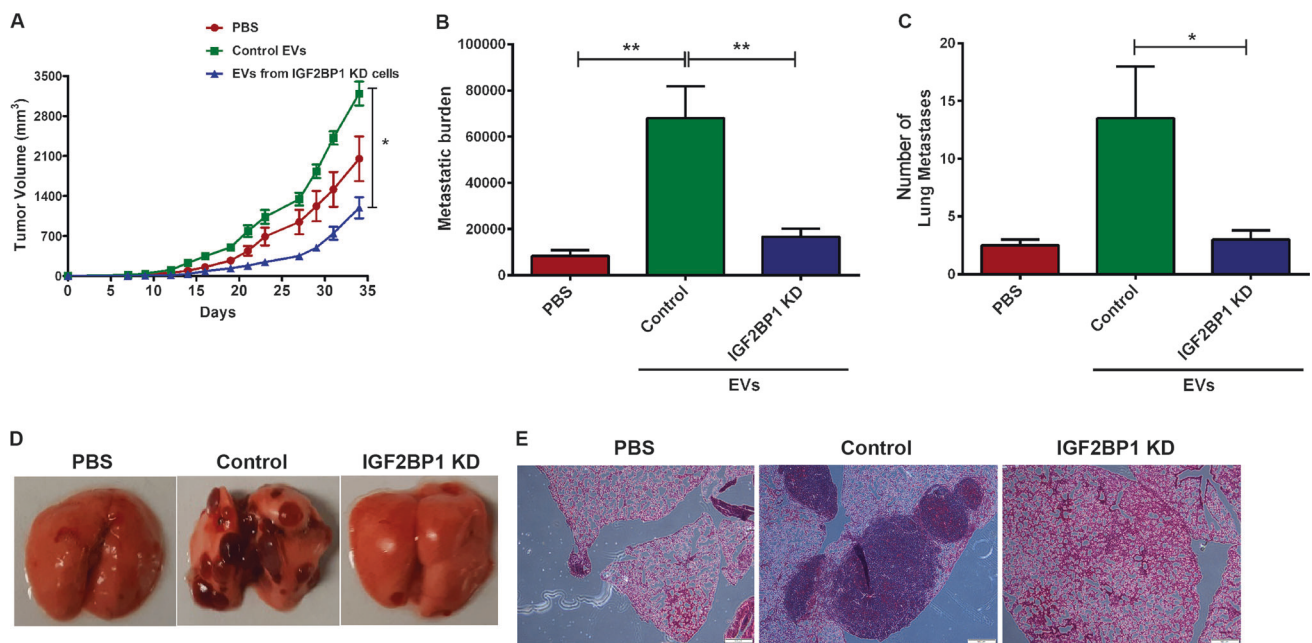


Fig. 3 **a** Analysis of primary tumor volume in C3H/HeJ mice injected with EVs (isolated with the sucrose cushion method) from control and IGF2BP1 knockdown cells over 35 days at an interval of 48 h; control group received PBS instead of EV injections. **b** Metastatic burden in each group calculated by determining the area of metastatic lesions in H&E-stained cross-sections of the lungs using ImageJ software. **c**

Number of lung metastatic lesions in each group. **d** Macroscopic imaging of lung metastasis in untreated mice and mice injected with either PBS or EVs from control or IGF2BP1 knockdown SW1 cells. **e** Microscopic analysis of lung metastasis after H&E staining of sectioned lung tissues of mice injected with either PBS or EVs from control or IGF2BP1 knockdown SW1 cells

negative control; it was abundantly detected in the cell lysates but was completely absent in the EVs, validating that the EVs were not contaminated with cellular material.

To further assess the role of IGF2BP1 in metastasis, wild-type IGF2BP1 (IGF2BP1^{WT}) was overexpressed in SW1 cells. As the construct had a green fluorescent protein (GFP) tag, we used a GFP plasmid as control. In addition, a GFP-tagged IGF2BP1 with a truncated KH domain (IGF2BP1^{dKH}) was transduced into SW1 cells to determine whether deletion of an RNA-binding domain could abrogate the function of the protein. TEM (Supplementary Fig. S10A) and NTA (Supplementary Fig. S10B) analyses showed that the size of EVs did not vary between the three groups. This was consistent with our previous results where the EVs from control and IGF2BP1 knockdown cells were in the same size range. Western blotting (Supplementary Fig. S10C) demonstrated the expression of exosomal marker CD81 as well as a prominent band corresponding to the size of GFP-tagged IGF2BP1 in the EVs from IGF2BP1^{WT}-overexpressed cells.

EVs mediate the role of IGF2BP1 in melanoma metastasis in vivo

To understand the function of IGF2BP1 in the EV-mediated effects on melanoma metastasis, the EVs isolated from the media of control and IGF2BP1 knockdown SW1 cells using

both methods of purification detailed in the Methods section were injected into separate groups of mice every alternate day over a period of 21 days. In addition to these two experimental groups, a third group of mice was injected with phosphate-buffered saline (PBS) instead of EVs. All groups were also injected subcutaneously on day 0 with parental SW1 cells, to initiate the primary tumor formation. The effects of the EVs on lung metastasis were nearly identical for both types of EV purification; Fig. 3 details the effects of the EVs purified with the sucrose cushion method, whereas Supplementary Fig. S11 shows the same for the EVs purified with general ultracentrifugation. Both Fig. 3a and Supplementary Fig. 11A reveal that the primary tumor volume was higher in the mice that received control EVs than the other two groups. Although this difference was significant, the effect of IGF2BP1 knockdown EVs was much more prominent on lung metastasis. As expected, EVs from the media of control SW1 cells dramatically increased metastasis compared with the PBS-treated group, revealing large metastatic lesions all over the lungs. Strikingly, the mice receiving EVs from the IGF2BP1 knockdown cells had little or no lung lesions as determined by metastatic burden (area of metastatic lesions in hematoxylin and eosin (H&E)-stained sections) and/or counting the number of metastatic lesions (Fig. 3b–e and Supplementary Fig. S11B–E). These in vivo results revealed that knocking down IGF2BP1 dramatically abrogated metastasis to the lungs.

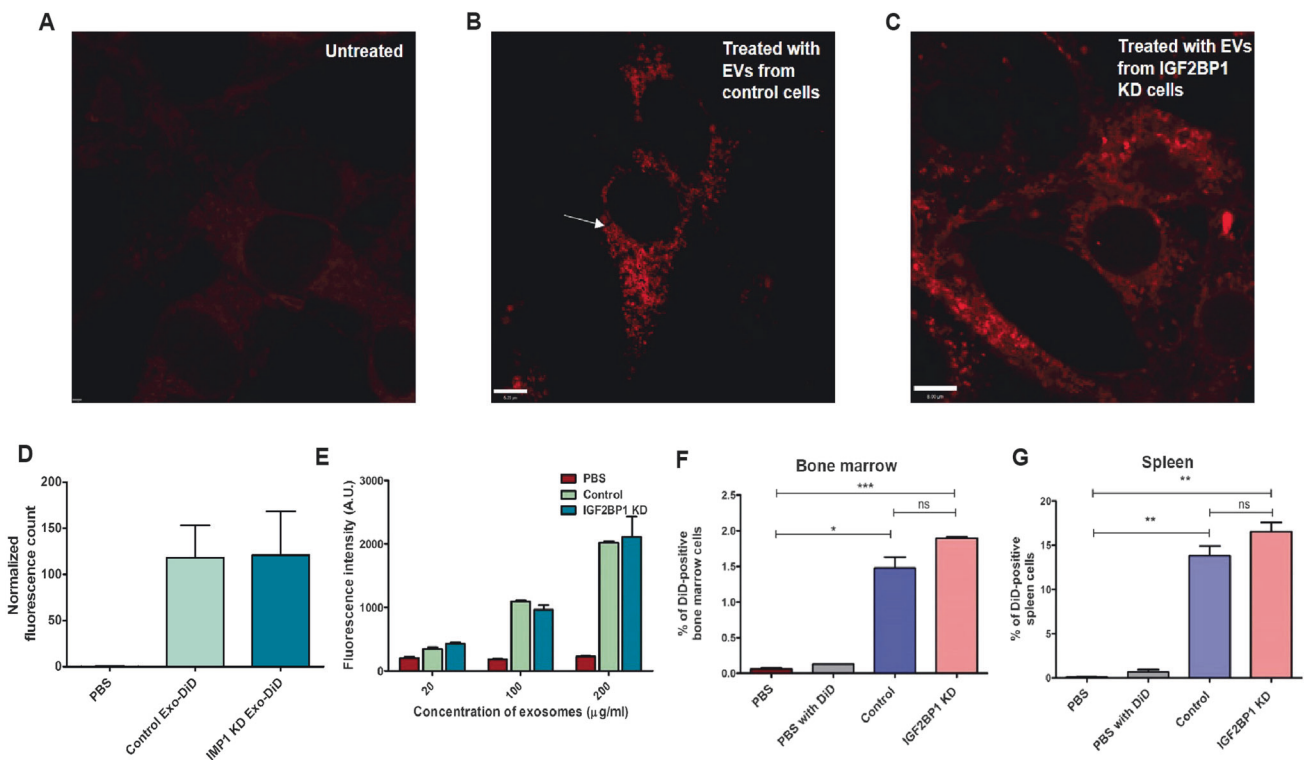


Fig. 4 Uptake of fluorescent DiD-labeled EVs isolated from control and IGF2BP1 knockdown cells. **a** Fixed untreated control NIH3T3 cells viewed under STED confocal microscope. **b, c** Fixed NIH3T3 cells viewed under STED confocal microscope to image uptake of DiD-labeled EVs following EV treatment for 24 h. **b** Cells treated with control EVs; larger sized EVs are distinctly visible and marked with arrows. **c** Cells treated with EVs from IGF2BP1 knockdown SW1 cells. **d** Quantitative analyses of images acquired in STED microscope. **e** Uptake of three different concentrations of EVs by

recipient NIH3T3 cells. Fluorescence intensity of the cells was measured in a fluorescence spectrometer, after 24 h of EV treatment. **f** Graphical representation of flow cytometric analysis of bone marrow cells isolated from mice that received tail vein injections of either PBS or DiD-PBS, or DiD-labeled EVs isolated from control or IGF2BP1 knockdown SW1 cells, 24 h before killing. **g** Graphical representation of flow cytometric analysis of splenic cells isolated from the same mice

In vivo administration of the EVs from IGF2BP1-overexpressed cells revealed that the percentage of mice bearing metastatic lung lesions was higher in IGF2BP1^{WT}-overexpressed group compared with the other groups (Supplementary Fig. S12A and B). The same can be visualized in Supplementary Fig. S12C showing H&E-stained cross-sections of the lungs. Intriguingly, the mice injected with EVs derived from the media of SW1 cells overexpressing RNA-binding mutant (IGF2BP1^{dKH}) did not develop metastatic lung lesions on par with the IGF2BP1^{WT} group, which suggested that RNA-binding capability is necessary for the EV-dependent effect of IGF2BP1 on metastasis. These data further confirm an important role for IGF2BP1 in EV-mediated melanoma metastasis.

Uptake of melanoma-derived EV in vitro and in vivo

As there was no difference in the size or concentration of EVs or protein isolated from the control and IGF2BP1 knockdown groups, we premised that there might be differential internalization of EVs between the two groups leading to the

difference in metastasis observed in our mouse model. In our in vitro experiment, uptake of fluorescent dye DiD-labeled EVs was visualized using the sub-diffraction imaging technique Stimulated Emission Depletion (STED) confocal microscopy. Distinct red spherical structures in the size range of EVs accumulated within the NIH3T3 cells, indicating the uptake of DiD-labeled EVs (Fig. 4a–c). Quantification of the normalized fluorescence is shown in Fig. 4d. Uptake by recipient NIH3T3 cells was in a dose-dependent manner, where the fluorescence intensity was directly proportional to the concentration of EVs uptaken (Fig. 4e). However, the recipient cells showed no preference in taking up the EVs from either the control or knockdown group.

Intravenous injection of DiD-labeled EVs into mice and collection of the organs after 24 h verified the result obtained in our in vitro cell culture experiment. Supplementary Fig. S13 shows the imaging of all the organs that were harvested for visualization of uptake of the labeled EVs. The lungs and liver exhibited higher retention of EVs after 24 h, which is in conformity with previously published literature [23]. Uptake of EVs by the other organs, viz. the

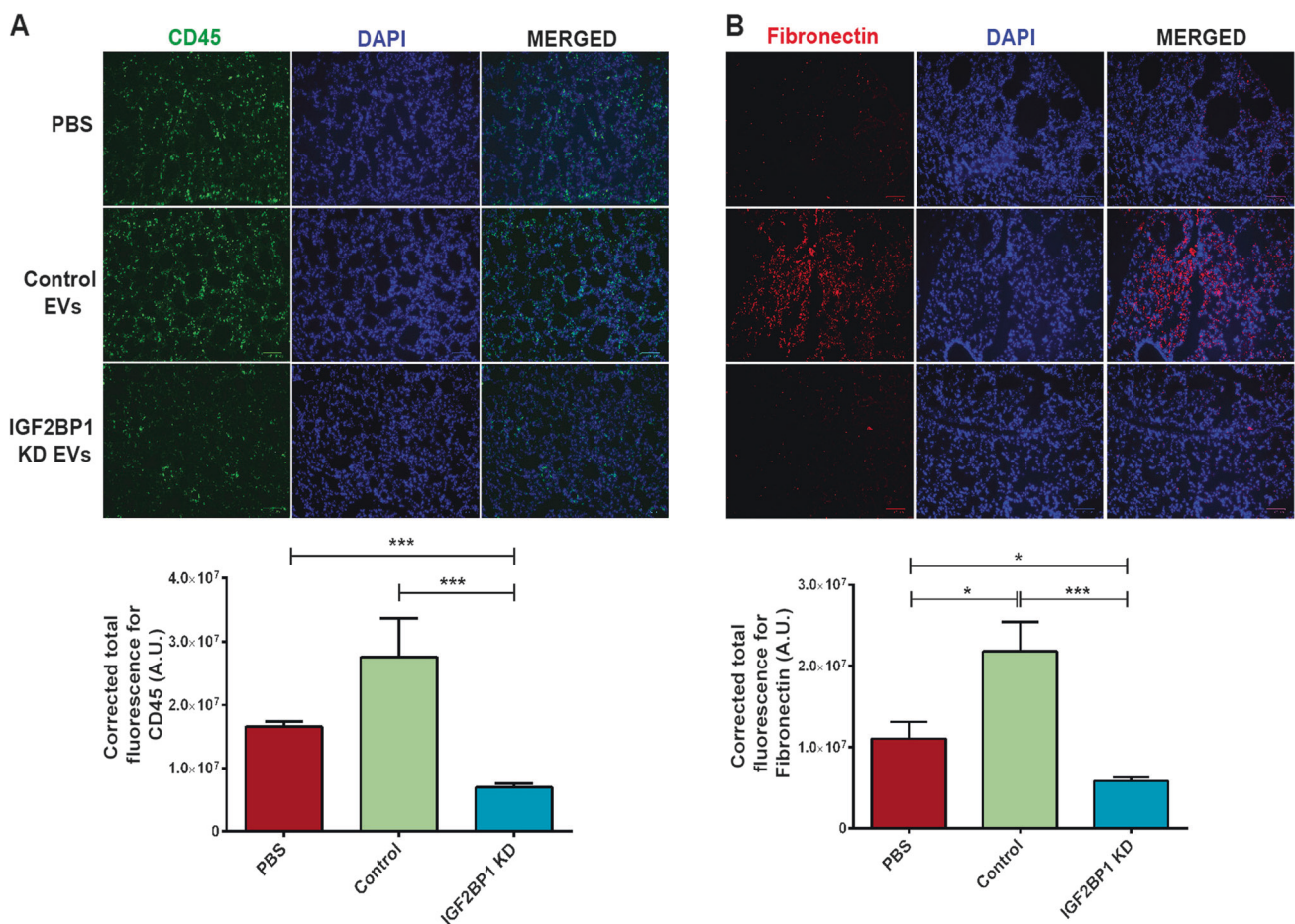


Fig. 5 Analysis of pre-metastatic niche formation in lungs. **a** Expression of CD45 (top panel) with quantitative analysis in the bottom panel. **b** Expression of fibronectin with quantitative analysis in the bottom panel. Expression of both CD45 and fibronectin increased

markedly in the lungs of the mice treated with EVs (isolated with the sucrose cushion method) from control SW1 cells, as compared with the mice that did not receive EVs or the mice that received EVs from IGF2BP1 knockdown SW1 cells. Scale bar is 100 μ m

heart, kidney, lymph node, and bone could not be visualized, which might have been because the percentage of cells taking up the EVs was not high enough for the IVIS imaging system to detect their fluorescence. Low-intensity fluorescence could be visualized in the spleen, which was congruous with the flow cytometry analysis, showing that ~14% of the splenic cells had taken up the EVs. DiD-labeled liposomes were taken up to some extent by the liver and showed a low signal, which was in agreement with previously published data [23]. EVs isolated from doxycycline-treated and untreated SW1 cells lacking the shIGF2BP1 construct were injected as controls. These EVs accumulated in the lungs of the mice after 24 h of injection. As the bone marrow and spleen are pivotal in pre-metastatic niche formation, we isolated single cells from the bone marrow and spleen of the mice and analyzed them for the internalization of fluorescent DiD-labeled EVs (Fig. 4f, g and Supplementary Fig. S14). Although there was a significant uptake of EVs by the spleen and bone marrow, there was no difference in uptake between the control and IGF2BP1

knockdown groups. EV biodistribution was distinctly visualized and quantified by the aforementioned in vitro and in vivo experiments, but there was no significant difference between the control and IGF2BP1 knockdown SW1 cells that could have affected metastasis.

Pre-metastatic niche formation

Given that exosomes have been reported to “educate” bone marrow-derived cells, our EV tissue biodistribution experiment, illustrating that the spleen and bone marrow were taking up EVs, led us to evaluate whether knocking down IGF2BP1 might have altered the “education” potential of the EVs. In this regard, we examined whether EVs promote a fibrotic microenvironment in the lungs and thereby recruit CD45⁺ cells. Using immunofluorescence, we found a pronounced increase in CD45 and fibronectin (Fig. 5a, b for sucrose cushion method and Supplementary Fig. S15A and B for general method of EV purification) in the lungs of the mice treated with EVs from control

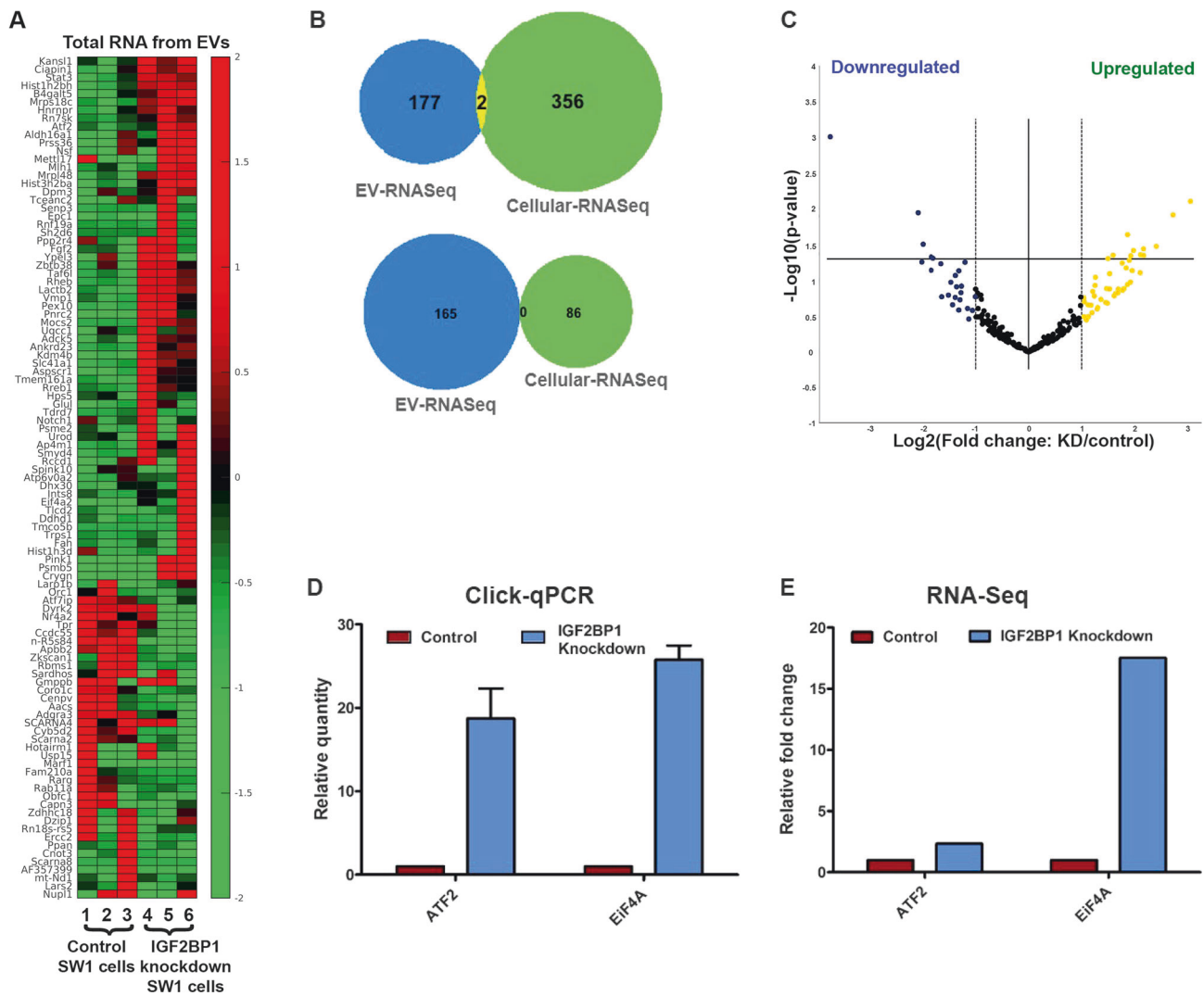


Fig. 6 **a** Heatmap analysis for sequencing of RNA from EVs. **b** Venn diagrams depicting overlap of RNA sequenced from SW1 cells as well as EVs from SW1 cells, either control or IGF2BP1 knockdown. Top: upregulated genes; bottom: downregulated genes. **c** Volcano plot showing microRNA sequencing analysis from EVs. **d**

Real-time PCR analysis to probe expressions of *ATF2* and *EIF4A2* genes in EU-labeled RNA from NIH3T3 cells treated with EVs derived from EU-labeled control and IGF2BP1 knockdown SW1 cells. **e** Graphical representation of the relative fold change of the same genes in the EVs as seen in the sequencing analysis of EVs

SW1 cells compared with the group that did not receive EVs. In contrast, the mice that received EVs from IGF2BP1 knockdown cells had markedly decreased fibronectin deposition and CD45⁺ cells. Graphical representations of quantified fluorescence are shown along with the images of fluorescence tissue sections.

To avoid possible cell line-specific artifacts, we have generated another mouse melanoma cell line, PVMM, with inducible CRISPR/Cas9-mediated knockout of IGF2BP1 (Supplementary Fig. S16A). Similar to the results obtained using SW1 cells in C3H mice, EVs isolated from IGF2BP1-deficient PVMM cells (western blotting characterization of EVs shown in Supplementary Fig. S16B) were less efficient than EVs from control cells in promoting development of pre-metastatic niche in the lungs of C57BL/6J mice, as

evidenced by infiltration by CD45-positive cells (Supplementary Fig. S16C). These data indicate that independent of the genetic background and melanoma cell line used, EVs mediate the role of IGF2BP1 in altering the lung micro-environment, which could influence melanoma metastasis.

RNA-sequencing

To examine the effects of IGF2BP1 suppression on the cargo of EVs, we performed a total gene expression profiling of the EVs. Heatmap (Fig. 6a) and Volcano plot (Supplementary Fig. S17A) representations show relative expression patterns of upregulated and downregulated genes. A list of all significantly altered genes is provided in Supplementary Table S1 (as a separate excel file). Analyses of the

differentially expressed genes using the Ingenuity software generated a number of pathways that were either activated or inhibited after knocking down IGF2BP1 (Supplementary Fig. S17B), which potentially contributed to the abrogation of pro-metastatic functions of the control EVs. Strikingly, comparing the cellular RNA with the EV-RNA showed little or no overlap (Fig. 6b), revealing that the abundance of a specific gene in the EVs did not directly correlate with its abundance in the parent cells. In our attempt to investigate whether specific motifs in genes might have influenced the differential loading of the genes into the EVs, we used the iRegulon software to generate motifs enriched in genes that were either upregulated or downregulated after IGF2BP1 knockdown. The top-scored motifs are illustrated in Supplementary Tables S2 and S3. In both tables, the areas under the cumulative recovery curve (AUCs) are reported on the second column, the normalized enrichment scores (NES) are presented on column 3 and genes with enriched motifs are listed on column 4. The 14 top motifs (including 7 for upregulated genes and 7 for downregulated genes) were discovered with NES > 4. The larger the NES and AUC scores, the more significant the motif enrichment is compared with the motifs in background genes. In addition, as EVs are known to carry microRNA (miRNA), a complete miRNA profiling was also done (list provided in Supplementary Table S4 as a separate excel file). Figure 6c depicts a volcano plot for the miRNAs that were upregulated or downregulated after suppressing IGF2BP1.

We further confirmed the uptake of EVs and transfer of RNA to recipient cells using click chemistry. We analyzed whether 5-ethynyl Uridine (EU)-labeled RNA from control and IGF2BP1 knockdown SW1 cells could be transferred by EVs to recipient NIH3T3 cells. Real-time PCR analysis of the EU-labeled RNA from recipient NIH3T3 cells demonstrated the uptake of EV-RNA. From the sequencing results, two genes—*ATF2* and *EiF4a2* (primer sequences are provided in Supplementary Table S5)—were probed based on their abundance and possible relevance to our study. Figure 6d depicts relative quantity of each gene in the EU-labeled cDNA pool isolated from recipient NIH3T3 cells. These expressions correlate with their expressions in the EVs (plotted in Fig. 6e) as observed in the sequencing studies.

Mass spectrometry analysis

Quantitative protein profiling of the EVs generated a number of proteins that were significantly altered after inhibiting IGF2BP1 (list of all proteins provided in Supplementary Table S6 as a separate excel file). Twenty-nine proteins were upregulated and 44 proteins were downregulated by more than 2-fold in the EVs from IGF2BP1

knockdown cells compared with control. Analysis of the proteomics results using the Ingenuity software generated canonical pathways that were possibly activated or repressed (Supplementary Fig. S17C) due to inhibition of IGF2BP1.

Discussion

Previous research has demonstrated that knocking down IGF2BP1 in melanoma cells in vitro inhibits cell proliferation, induces apoptosis [11], and sensitizes the cells to chemotherapeutic or inhibitory agents [12, 24]. However, to our knowledge, the role of IGF2BP1 in melanoma metastasis has been hitherto unexplored. Although there are reports implicating IGF2BP1 in the metastasis of glioblastoma [25] and cervical cancer [26], its role in the interplay between tumor cells and the tumor microenvironment leading to melanoma metastasis is a complex process that needs a detailed investigation.

Herein we present for the first time the effects of IGF2BP1 on EVs secreted by melanoma cells, which in turn impacts metastatic events in vivo. In this pursuit, we used two different mouse models to test our hypothesis that suppressing IGF2BP1 might have a negative impact on primary melanoma tumor formation. Interestingly, contrary to our hypothesis, primary tumors developed similarly in both the control and IGF2BP1-suppressed groups. However, both genetic deletion and short hairpin RNA (shRNA)-mediated inducible knockdown of IGF2BP1 drastically inhibited melanoma metastasis.

As cancer cells have been typically known to communicate via direct cellular contact and the secretion of certain soluble factors such as cytokines, we pursued some avenues whereby IGF2BP1 might have affected the pro-metastatic intrinsic properties or the cytokine/chemokine secretion profiles of the cells in vitro. However, we insinuated from our experiments that there is no difference between the control and IGF2BP1 knockdown groups. Therefore, we considered the possibility that IGF2BP1 might regulate other extracellular secretory factors interacting with the tumor microenvironment to affect metastasis. This led us to explore the emerging field of tumor-secreted EVs, which has transpired as a key contributor to cancer metastasis.

We characterized and performed our in vivo metastasis and niche formation experiments with EVs purified using the standard differential ultracentrifugation as well as a previously established sucrose cushion-based ultracentrifugation method. Both methods yielded similar and reproducible results in our in vivo experiments, with the latter incorporating a sucrose cushion for purification of EVs to reduce contaminating non-vesicular components.

However, there is a possibility that contaminating non-vesicular components were still present with the EVs, which could have contributed toward the *in vivo* phenotype described herein.

Consistent with the earlier reports [14], we observed that the EVs from control melanoma cells contributed significantly to primary tumor growth, possibly because the EVs contributed to the recruitment of bone marrow-derived cells to the primary tumor. Intriguingly, EVs from IGF2BP1 knockdown cells inhibited the primary tumor development. The EVs had a similar, yet dramatically more pronounced effect on lung metastasis. Mice injected with EVs from control melanoma cells had dramatically increased lung metastasis, whereas EVs from the IGF2BP1 knockdown melanoma cells drastically reduced the metastatic lung lesions. This study is the first to reveal that IGF2BP1 affects EVs in some manner to influence melanoma metastasis. Delving into the possible reasons behind this effect revealed no differences in the size, number, or protein/RNA concentration of the EVs secreted by control and IGF2BP1 knockdown SW1 cells.

As organotropic homing of exosomes has been associated with metastasis [27], we exploited fluorescently labeled EVs to assess their *in vivo* biodistribution profile. However, suppressing IGF2BP1 did not affect the tropism of the EVs, which could be because the repertoire of surface integrins, which has been shown to regulate tropism [27], was not modulated by IGF2BP1. Although the bone marrow and spleen did not differentially uptake the EVs derived from the control and IGF2BP1-downregulated SW1 cells, they were of particular importance. This is because exosomes have been shown to interact with bone marrow-derived cells to contribute to pre-metastatic niche formation [14, 19, 20]. Studies in different tumor models have shown augmented fibronectin deposition in pre-metastatic niches, which in turn recruits bone marrow-derived macrophages and neutrophils [20, 28–30]. Consistent with this paradigm, we showed that EVs from control SW1 cells elicited fibronectin deposition and elevated the number of CD45⁺ cells in lungs. In striking contrast, the mice treated with EVs derived from IGF2BP1-downregulated cells displayed much less fibronectin deposition and fewer CD45⁺ cells in the lungs, which was found to be on par with the mice that received no EVs at all. Our observations demonstrate that EVs orchestrate the critical role of IGF2BP1 in modifying distant microenvironments, thereby explaining why down-regulating IGF2BP1 had abrogated melanoma metastasis in our earlier experiments.

Although multiple reports have correlated the differential cellular expression of certain genes or proteins with a difference in size, production, or RNA/protein content of exosomes [31, 32], in our study we found that IGF2BP1 has

no such effect on the secreted EVs. Nor did we find a difference in organotropism of EVs after suppression of IGF2BP1. However, a comprehensive RNA and protein analysis of the EVs revealed an extensive differential loading of many mRNA, snRNA, miRNA, and protein molecules in the EVs between the control and IGF2BP1 knockdown groups. This provided us with interesting insights into the pathways that might be impacted by knocking down IGF2BP1. The fact that loading of genes in the EVs did not correlate with their abundance in the SW1 cells indicated that this could be a well-regulated process in which IGF2BP1 might play a direct or indirect role. The enrichment of certain motifs in the genes differentially expressed after suppression of IGF2BP1 could be a plausible explanation for the differential loading. However, further studies are necessary for better comprehension of this mechanism. On the basis of these data, we propose that the dramatic abrogation of melanoma metastasis by suppression of IGF2BP1 was due to its pronounced effect on the cargo of the EVs. Further investigations into the pathways could provide a detailed understanding of the effect of IGF2BP1 on the content of EVs. Furthermore, we confirmed the transfer of several RNA molecules from parent cells via EVs to recipient cells by using the unique click chemistry. This chemistry may be further exploited for a thorough investigation of EV-mediated transfer of genes *in vivo*.

To the best of our knowledge, our study is the first to report that the RNA-binding protein IGF2BP1 plays a critical role in melanoma metastasis. It is also the first to demonstrate the role of an RNA-binding protein in EV-mediated promotion of metastasis. Collectively, our results identify that EVs within 150 nm of diameter mediate the effects of suppression of IGF2BP1 *in vivo*. Suppression of this protein modulates the cargo of the EVs, suppressing pre-metastatic niche formation and inhibiting melanoma metastasis. As patient survival in most cancers is directly dependent on tumor metastasis, targeting IGF2BP1 could potentially open up novel avenues for the development of inhibitors of melanoma metastasis.

Materials and methods

Cell culture

Mouse melanoma cell lines SW1 and PVMM were obtained as generous gifts from Dr. Ze'ev Ronai of Sanford Burnham Prebys Medical Discovery Institute and Dr. Serge Y. Fuchs of University of Pennsylvania, respectively. Cells were maintained as monolayers in Dulbecco's modified Eagle's medium (DMEM; VWR International), supplemented with 10% v/v fetal bovine serum (FBS, Gibco by Life

Technologies), 100 IU of Penicillin G and 100 µg/ml Streptomycin (Corning). The cell lines were tested for mycoplasma contamination with MycoAlert Plus Mycoplasma detection kit (Lonza).

Generation of IGF2BP1 knockdown melanoma cell lines

IGF2BP1 was knocked down using either of two different lentiviral, inducible shRNA constructs—pInducer24 and M1 in SW1 mouse melanoma cell line. pInducer24 has a previously published mouse IGF2BP1-specific shRNA [6] in a pInducer11 vector backbone [33]. M1 (purchased from Genecopoeia) has the shRNA construct (target sequence: 5'-GATCCGCAATATTCCACCT-3') in a psi-LVRInU6TGP vector backbone. Alternatively, IGF2BP1 was knocked out with CRISPR-Cas9 technology using inducible Cas9 (GE Dharmacon) and constitutive gRNA (Genecopoeia; target sequence: 5'-GAGTGTGACCCCCGCAGACT-3'). Ten micrograms of the expression vector (pInducer24 or M1), 10 µg of packaging vector pPAX, and 7.5 µg of envelop plasmid pMD.G were used to produce viral particles in 293T cells as previously described. SW1 or PVMM cells were transduced in the presence of 8 µg hexadimethrine bromide (polybrene; Sigma), followed by a single-cell sorting and selection of clones with efficient IGF2BP1 knockdown. In vitro, expression of inducible plasmids (either IGF2BP1 shRNA or Cas9) was induced by 1–2 µg/ml of doxycycline for 4–8 days.

Western blotting

Western blotting was done with previously established protocol, with a few modifications [34, 35]. Cells were lysed using RIPA buffer (Sigma-Aldrich) combined with Halt™ Phosphatase Inhibitor Cocktail (Thermo Scientific). Lysates were then vortexed and cleared by spinning at 15,000 × g for 10 min at 4 °C. Protein concentration was determined using DC Protein Assay (Bio-Rad) and lysates were separated by electrophoresis on a 10% SDS-polyacrylamide gel. Proteins were then transferred onto a nitrocellulose membrane at 100 V for 1 h, then blocked with Tris-buffered saline/0.1% Tween 20 containing 5% non-fat dry milk for 1 h. The membranes were probed overnight at 4 °C with primary antibody, washed, and subsequently incubated with secondary antibodies for 1 h at room temperature. Anti-IGF2BP1 and anti β-actin primary antibodies were obtained from Cell Signaling Technology (CST; catalog number D33A2 and 13E5, respectively) and used at a dilution of 1:1000. Horseradish peroxidase-conjugated secondary antibody, procured from CST, was used at a dilution of 1:2000 (anti-rabbit secondary IgG #7074).

Reverse transcription and (quantitative) real-time PCR

Total RNA was isolated from cells using the RNeasy Mini Kit (Qiagen) according to the manufacturer's instructions. cDNA was generated using iScript™ cDNA Synthesis Kit (Bio-Rad), following the manufacturer's protocol. cDNA was amplified by real-time PCR using iTaq™ Universal SYBR® Green Supermix (Bio-Rad) on a Bio-Rad CFX96 Touch™ Real-Time PCR Detection System. The analysis was performed on each sample in triplicate. Relative transcript levels were calculated using the comparative Ct method and normalized to the previously characterized housekeeping gene *RPS18*. Primer sequences are described in Supplementary Table S5.

Genetically engineered in vivo metastasis model

Animal procedures were conducted in accordance with conditions approved by Institutional Animal Care and Use Committee, Pennsylvania State University College of Medicine. BRaf^{CA}, Tyr::CreER, Pten^{lox4-5} and BRaf^{CA}, Tyr::CreER, Pten^{lox4-5}, IGF2BP1^{loxP-loxP} mice were genotyped as previously described [36]. Cre-mediated conversion of BRaf^{CA} to BRaf^{VE}, deletion of exons 4 and 5 of Pten, and knockout of IGF2BP1 were assessed by PCR as previously reported. For localized melanoma induction on the back skin, 6- to 8-week-old mice (both male and female) were treated topically with 2 µl of 1.9 mg/ml (5 mM) 4-hydroxytamoxifen (4-HT). Twenty-five to 50 mg/ml (65–130 mM) 4-HT solution was prepared by dissolving 4-HT (70% Z-isomer, Sigma) in dimethyl sulfoxide. Generalized induction in adult mice was performed by intraperitoneal injection of 1 mg of tamoxifen/40 g mouse for 3 consecutive days. In this case, tamoxifen was prepared as a 10 mg/ml suspension in peanut oil. Body weight and tumor size were measured twice a week and tumor volume was calculated based on the following formula: volume = length (mm) × [width² (mm²)/2]. It should be mentioned here that the survival graphs plotted do not depict the true survival of all the mice in each group, as we had to kill the mice that had reached the maximum permissible tumor size and consider the day of killing as the end point.

Syngeneic tumorigenic and metastasis model

Six to 8-week-old male and female C3H/HeJ mice from The Jackson Laboratory were used for subcutaneous injection of SW1 cells transduced with shRNA against IGF2BP1. The C3H/HeJ mice were injected with SW1 cells engineered to have doxycycline-inducible expression of IGF2BP1-specific shRNA (shIGF2BP1). Two different shRNA

constructs—pInducer24 and M1—were used separately in our *in vivo* experiments. Cells (1×10^6) were suspended in PBS and injected into the right flank of mice. Five days after injection, knockdown was induced *in vivo* by treating mice with doxycycline pellet. This treatment was maintained throughout the length of the experiment. Body weight and tumor size were measured three times a week and tumor volume was calculated based on the following formula: volume = length (mm) \times [width² (mm²)/2].

Migration and invasion assays

Cell migration assays were performed using Radius™ 24-Well Cell Migration assay Kit (Cell Biolabs, Inc.) as per the manufacturer's protocol. Briefly, SW1 cells were treated for 48 h with doxycycline to induce IGF2BP1 knockout and seeded on pre-treated Radius™ 24-well cell migration plate (Cell Biolabs, Inc.) at 1.0×10^5 /well for 12 h. When cells reached 85% confluency, plates were treated with Radius™ gel removal solution to expose the cell-free areas to cell migration. Cells were allowed to migrate for 24 h and compared with SW1 cells that were not treated with doxycycline. Invasion assays were performed using BD Bio-Coat Matrigel Invasion Chamber (BD Biosciences). SW1 cells, with or without doxycycline treatment, were prepared in triplicate at 5×10^4 cells/insert in serum-free DMEM media containing all supplements. A 10% *v/v* FBS (Gibco) media was used as a chemoattractant. Plates were incubated for 24 h at 37 °C in 5% CO₂, after which the invading cells were fixed, stained, and mounted onto microscope slides.

Intravenous injection of cancer cells in mice

C3H mice ($n \geq 12$) were *i.v.* injected with 1×10^6 SW1 cells. Lungs were analyzed for metastasis 35 days after injection. The experiment was repeated at least three times. Approximately equal number of male and female mice were assigned randomly to each group for all *in vivo* experiments reported in this study. No blinding was done for any of the mice experiments.

RNA-seq analysis

Three biological replicates of control and IGF2BP1 knockdown cells were collected and RNA was isolated using Rneasy Mini Kit (Qiagen) before being subjected to mRNA sequencing.

Cytokine profiling

Culture media from control and IGF2BP1 knockdown SW1 cells were collected and sent to UPCI Cancer

Biomarkers Facility: Luminex Core Laboratory (Pittsburg, PA) for profiling a panel of 32 cytokines.

Purification of EVs from IGF2BP1-depleted and -overexpressed cell lines, and their characterization

EVs were isolated from five different derivatives of the SW1 mouse melanoma cell line for inducible shRNA-mediated knockdown (as before) as well as overexpression of IGF2BP1. Overexpression of IGF2BP1 was achieved by transducing SW1 cells with GFP-tagged IGF2BP1^{WT} plasmid. Separately, SW1 cells were transduced with GFP-tagged IGF2BP1^{dKH} plasmid, which has a deleted RNA-binding KH domain [37]. GFP plasmid was used as a control. EVs were also isolated from control and IGF2BP1-knockout PVMM cells.

All cell lines were plated in complete media with 10% FBS and cultured for 24 h. Thereafter, the media were replaced by DMEM without FBS and maintained for 48 h, at the end of which EVs were collected from the culture media. Induction of IGF2BP1 knockdown was done in SW1 cells with doxycycline in serum-free media for the 48 h time period before collection of culture media. Culture media were subjected to centrifugation at $2000 \times g$ for 30 min to eliminate dead cells, followed by ultracentrifugation at $20,000 \times g$ for 30 min to eliminate cell debris. The supernatants from this step were spun at $100,000 \times g$ for 2 h in the ultracentrifuge. The pellets from this step were washed with PBS in another round of ultracentrifugation at $100,000 \times g$ for 2 h. The pellets were then resuspended in 1 ml of PBS for every 60 ml of starting culture media. Alternatively, a sucrose cushion method was used to obtain EVs of greater purity, where 30% sucrose was used to pellet out purified EVs [38]. The EVs were characterized using NTA, TEM, and western blottings for the analysis for specific exosomal markers, viz., CD81 (Santa Cruz Biotechnology #sc-166029), HSP70 (CST #4872), Alix (CT #2171), and TSG101 (Santa Cruz Biotechnology #sc-7964) as well as golgi marker GM130 (Novus Biologicals #NBP2-53420). Starting cellular lysates were also analyzed for the same to demonstrate an enrichment of the exosomal markers in the EVs in comparison with cell lysates. Concentration of the EVs was measured using Nanodrop (Thermo Scientific).

Injection of C3H/HeJ mice with EVs

EVs isolated using both methods of purification were administered via tail vein injections in separate experiments at a concentration of 10 μ g (by protein) in 100 μ l of PBS per mouse, followed by subcutaneous injection of SW1 cells (0.7×10^6 cells per mouse) into the flank of each mouse. Over the next 21 days, the same concentration of EVs was

injected into the mice on alternate days. EVs from the five different transduced cell lines mentioned above were injected into the mice. The control group received 100 μ l of PBS without EVs. Primary tumor and body weight measurements were done every alternate day, for 35 days. At the end of the 35-day time period, the mice were killed and their lungs were collected for analysis of tumor metastasis to the lungs. Metastatic lung lesions were counted, before the lungs were sectioned for staining with H&E to facilitate microscopic analysis. Thirteen mice were kept in each of the control and knockdown groups, and six mice were kept in each of the groups for the IGF2BP1 overexpression experiment. The experiment was repeated three times with $n = > 8$ each time.

In vitro uptake of fluorescent DiD-labeled EVs

NIH3T3 cells were plated in a 96-well plate at a density of 5000 cells/well in triplicate. The experiment was repeated three times. After allowing the cells to attach for 8 h, the media were replaced with serum-free media containing EVs at various concentrations, after washing the cells with PBS. EVs from control and IGF2BP1 knockdown SW1 cells were labeled with fluorescent dye DiD by incubating the EVs with DiD at a concentration of 5 μ g/ml in PBS for 15 min at room temperature. Thereafter, the EVs were washed with PBS by centrifuging at 100,000 $\times g$ for 2 h and used for treatment of the NIH3T3 cells. After 24 h of treatment with EVs, the EV-containing media were discarded and the cells were washed three times with PBS. Thereafter, the fluorescence intensity of the cells was recorded in a multi-mode microplate reader (CLARIOstar) at an excitation wavelength of 640 nm and an emission wavelength of 670 nm. NIH3T3 cells were also imaged in a STED confocal microscopy (Leica) to visualize the uptake of the DiD-labeled EVs. The same treatment conditions were followed as above.

In vivo biodistribution of EVs

Twenty micrograms of DiD-labeled EVs were injected via tail vein into each C3H/HeJ mouse. Twenty-four hours after the injection, the mice were killed and the organs were collected. The organs were imaged with an IVIS Lumina Series III Imaging System (PerkinElmer) to detect the fluorescence of DiD-labeled EVs uptaken by the organs. The imaging for PBS, control, and IGF2BP1 groups were repeated twice with $n = > 3$ mice per group. The spleen and bone marrow cells were isolated from each mouse and single-cell suspensions were prepared. Each sample was then run in a flow cytometer and cells with the DiD-labeled EVs were detected in the Allophycocyanin (APC) channel with red laser excitation. One hundred nanometer liposomes (Encapsula NanoSciences LLC) were also labeled with DiD and injected into the mice

as control. Furthermore, EVs from parent SW1 cells (without the shIGF2BP1) were used as controls for this experiment, with or without doxycycline treatment.

Fluorescent detection in immunohistochemistry of lung tissue

To detect the contribution of EVs toward the formation of metastatic niche in vivo, lung tissues were probed for the differential expression of fibronectin and CD45 in the C3H/HeJ or C57BL/6J (The Jackson Laboratory) mice receiving either PBS or EVs isolated from control or IGF2BP1-depleted SW1 or PVMM (syngeneic to C57BL/6J mice) cells, respectively. EVs were isolated from SW1 cells with either method of purification mentioned above. The mice were treated with 20 μ g of EVs per mouse via tail-vein injection every alternate day for a period of 21 days. The mice were killed 1 week after the last EV injection and their lungs were collected. The 4% paraformaldehyde-fixed lung tissues were paraffin-embedded and sectioned, after which fluorescence immunohistochemistry was performed. In brief, the sections were deparaffinized and antigen retrieval was done with TE buffer (pH9) and 10 mM citrate buffer (pH 6) for fibronectin and CD45, respectively. Following blocking, the lung tissue sections were incubated overnight with primary antibodies against fibronectin (Abcam #ab2413) or CD45 (Novus Biologicals #AF114). Fluorescently labeled secondary antibodies (Jackson Laboratories) were used in conjunction with nuclear dye DAPI (4',6-diamidino-2-phenylindole) to visualize the distribution of fibronectin and CD45 in the lung tissues. The in vivo experiment was repeated twice.

RNA-seq and analysis

EVs were isolated from control and IGF2BP1 knockdown SW1 cells. RNA were isolated from the EVs (in three biological replicates) using TRIzol Reagent (Life technologies), followed by the Direct-ZolTM RNA Miniprep Plus (Zymo Research) kit, according to the manufacturer's instructions. The RNA samples were then subjected to total as well as miRNA sequencing in triplicates. Ingenuity software (Qiagen) was used to analyze the RNA-seq results and generate possible pathways/genes affected by knocking down IGF2BP1. We detected motifs enriched in the upregulated as well as the downregulated genes identified from the RNA-seq of EVs, using the iRegulon software (<http://iregulon.aertslab.org/>) in Cytoscape (<http://www.cytoscape.org/>).

Transfer of RNA to recipient cells via EVs

To detect the transfer of EVs from parent cells to recipient cells in vitro, the Click-iT Nascent RNA Capture kit (Life

Technologies), which is based on labeling of nascent RNA with the uridine analog 5-EU, was exploited [39]. Control and IGF2BP1 knockdown SW1 cells were treated with 0.2 mM 5-EU for 24 h, after which EVs were isolated from the cell culture media as before. These EVs from control and knockdown SW1 cells were then added separately on to recipient NIH3T3 cells. After 24 h of treatment with EVs, the cells were collected and total RNA was isolated with RNeasy Mini kit (Qiagen). Subsequently, from this total RNA prep, 5-EU-labeled RNAs were pulled down using the Click-iT Nascent RNA Capture kit, following the manufacturer's protocol. In brief, 5 µg of RNA was biotinylated and precipitated using the Click chemistry. These steps were followed by binding of 1 µg of the biotinylated RNA to Dynabead MyOne Streptavidin T1 magnetic beads (Thermo Fisher Scientific) and subsequent wash steps to eliminate the possibility of nonspecific binding. The EU-RNA bound to the beads were used as a template for cDNA synthesis. In the final step, the freshly synthesized cDNA was released from the beads and used for subsequent real-time PCR analyses using SYBR Green and gene-specific primers.

Mass spectrometry

EVs were isolated as above. Protein profiling and comparative analysis was done by MS Bioworks LLC (Ann Harbor, MI). After in-gel trypsin digestion, each sample was analyzed by nano liquid chromatography tandem mass spectrometry using nanoACQUITY high-performance liquid chromatography system (Waters Incorporated, Charlotte, NC) interfaced with a Q Exactive Quadrupole-Orbitrap (ThermoFisher Scientific). Data were searched using MASCOT database, which were then fed into the Scaffold software for analysis. Ingenuity software (Qiagen) was used for analysis of the mass spectrometry results and generate pathways/proteins possibly affected by knocking down IGF2BP1.

Statistical analysis

The experimental results are representative of replicates as mentioned in the Materials and Methods section. Data are presented as mean ± SEM. Statistical analyses were carried out using GraphPad Prism software. Unpaired two-tailed Student's *t*-tests and one-way analysis of variance were performed to compare two groups and three groups, respectively. Statistically significant differences are indicated on the graphs by asterisk symbols (* $P < 0.05$; ** $P < 0.01$; *** $P < 0.001$).

Acknowledgements This study was supported in part by the NIH grant R01 AR063361 (VSS). We thank Dr Ze'ev Ronai for the generous gift of reagents and Dr JM Sundstrom for the help with

Nanosight™ analysis of EVs. We thank Penn State Cancer Institute Genomics Sciences, Penn State College of Medicine Imaging Core, Flow Cytometry Core, and Molecular and Histopathology Core Facilities for help with respective data acquisition and analysis.

Compliance with ethical standards

Conflict of interest The authors declare that there is no conflict of interest.

Publisher's note: Springer Nature remains neutral with regard to jurisdictional claims in published maps and institutional affiliations.

References

- Dimitriadis E, Trangas T, Milatos S, Foukas PG, Gioulbasanis I, Curtis N, et al. Expression of oncofetal RNA-binding protein CRD-BP/IMP1 predicts clinical outcome in colon cancer. *Int J Cancer*. 2007;121:486–94.
- Bell JL, Turlapati R, Liu T, Schulte JH, Huttelmaier S. IGF2BP1 harbors prognostic significance by gene gain and diverse expression in neuroblastoma. *J Clin Oncol*. 2015;33:1285–93.
- Vikesaa J, Hansen TV, Jonson L, Borup R, Wewer UM, Christiansen J, et al. RNA-binding IMPs promote cell adhesion and invadopodia formation. *EMBO J*. 2006;25:1456–68.
- Elcheva I, Goswami S, Noubissi FK, Spiegelman VS. CRD-BP protects the coding region of betaTrCP1 mRNA from miR-183-mediated degradation. *Mol Cell*. 2009;35:240–6.
- Goswami S, Tarapore RS, Poenitzsch Strong AM, TeSlaa JJ, Grinblat Y, Setaluri V, et al. MicroRNA-340-mediated degradation of microphthalmia-associated transcription factor (MITF) mRNA is inhibited by coding region determinant-binding protein (CRD-BP). *J Biol Chem*. 2015;290:384–95.
- Noubissi FK, Elcheva I, Bhatia N, Shakoori A, Ougolkov A, Liu J, et al. CRD-BP mediates stabilization of betaTrCP1 and c-myc mRNA in response to beta-catenin signalling. *Nature*. 2006;441:898–901.
- Noubissi FK, Goswami S, Sanek NA, Kawakami K, Minamoto T, Moser A, et al. Wnt signaling stimulates transcriptional outcome of the Hedgehog pathway by stabilizing GLI1 mRNA. *Cancer Res*. 2009;69:8572–8.
- Sparanese D, Lee CH. CRD-BP shields c-myc and MDR-1 RNA from endonucleolytic attack by a mammalian endoribonuclease. *Nucleic Acids Res*. 2007;35:1209–21.
- Leeds P, Kren BT, Boylan JM, Betz NA, Steer CJ, Gruppiso PA, et al. Developmental regulation of CRD-BP, an RNA-binding protein that stabilizes c-myc mRNA in vitro. *Oncogene*. 1997;14:1279–86.
- Stohr N, Huttelmaier S. IGF2BP1: a post-transcriptional “driver” of tumor cell migration. *Cell Adh Migr*. 2012;6:312–8.
- Elcheva I, Tarapore RS, Bhatia N, Spiegelman VS. Overexpression of mRNA-binding protein CRD-BP in malignant melanomas. *Oncogene*. 2008;27:5069–74.
- Craig EA, Spiegelman VS. Inhibition of CRD-BP sensitizes melanoma cells to chemotherapeutic agents. *Pigment Cell Melanoma Res*. 2012;25:83–7.
- Kim T, Havighurst T, Kim K, Albertini M, Xu YG, Spiegelman VS. Targeting insulin-like growth factor 2 mRNA-binding protein 1 (IGF2BP1) in metastatic melanoma to increase efficacy of BRAF(V600E) inhibitors. *Mol Carcinog*. 2018;57:678–83.
- Peinado H, Alečković M, Lavotshkin S, Matei I, Costa-Silva B, Moreno-Bueno G, et al. Melanoma exosomes educate bone marrow progenitor cells toward a pro-metastatic phenotype through MET. *Nat Med*. 2012;18:883.

15. Azmi AS, Bao B, Sarkar FH. Exosomes in cancer development, metastasis, and drug resistance: a comprehensive review. *Cancer Metastas- Rev.* 2013;32:623–42.
16. Chen Y, Zeng C, Zhan Y, Wang H, Jiang X, Li W. Aberrant low expression of p85alpha in stromal fibroblasts promotes breast cancer cell metastasis through exosome-mediated paracrine Wnt10b. *Oncogene.* 2017;36:4692–705.
17. Weidle HU, Birzele F, Kollmorgen G, RÜGer R. The multiple roles of exosomes in metastasis. *Cancer Genom Proteom.* 2017;14:1–16.
18. Lobb RJ, Lima LG, Moller A. Exosomes: key mediators of metastasis and pre-metastatic niche formation. *Semin Cell Dev Biol.* 2017;67:3–10.
19. Hood JL, San RS, Wickline SA. Exosomes released by melanoma cells prepare sentinel lymph nodes for tumor metastasis. *Cancer Res.* 2011;71:3792–801.
20. Costa-Silva B, Aiello NM, Ocean AJ, Singh S, Zhang H, Thakur Basant K, et al. Pancreatic cancer exosomes initiate pre-metastatic niche formation in the liver. *Nat Cell Biol.* 2015;17:816.
21. Dankort D, Curley DP, Cartledge RA, Nelson B, Karnezis AN, Damsky WE Jr., et al. Braf(V600E) cooperates with Pten loss to induce metastatic melanoma. *Nat Genet.* 2009;41:544–52.
22. Hamilton KE, Noubissi FK, Katti PS, Hahn CM, Davey SR, Lundsmith ET, et al. IMP1 promotes tumor growth, dissemination and a tumor-initiating cell phenotype in colorectal cancer cell xenografts. *Carcinogenesis.* 2013;34:2647–54.
23. Wen SW, Sceneay J, Lima LG, Wong CS, Becker M, Krumeich S, et al. The biodistribution and immune suppressive effects of breast cancer-derived exosomes. *Cancer Res.* 2016;76:6816–27.
24. TaeWon K, Thomas H, KyungMann K, Mark A, G XY, S SV. Targeting insulin-like growth factor 2 mRNA-binding protein 1 (IGF2BP1) in metastatic melanoma to increase efficacy of BRAFV600E inhibitors. *Mol Carcinog.* 2018;57:678–83.
25. Wang R-j, Li J-w, Bao B-h, Wu H-c, Du Z-h, Su J-l, et al. MicroRNA-873 (miRNA-873) inhibits glioblastoma tumorigenesis and metastasis by suppressing the expression of IGF2BP1. *J Biol Chem.* 2015;290:8938–48.
26. Su Y, Xiong J, Hu J, Wei X, Zhang X, Rao L. MicroRNA-140-5p targets insulin like growth factor 2 mRNA binding protein 1 (IGF2BP1) to suppress cervical cancer growth and metastasis. *Oncotarget.* 2016;7:68397–411.
27. Hoshino A, Costa-Silva B, Shen T-L, Rodrigues G, Hashimoto A, Tescic Mark M, et al. Tumour exosome integrins determine organotrophic metastasis. *Nature.* 2015;527:329.
28. Liu Y, Gu Y, Han Y, Zhang Q, Jiang Z, Zhang X, et al. Tumor exosomal RNAs promote lung pre-metastatic niche formation by activating alveolar epithelial TLR3 to recruit neutrophils. *Cancer Cell.* 2016;30:243–56.
29. Peinado H, Lavotshkin S, Lyden D. The secreted factors responsible for pre-metastatic niche formation: old sayings and new thoughts. *Semin Cancer Biol.* 2011;21:139–46.
30. Psaila B, Lyden D. The metastatic niche: adapting the foreign soil. *Nat Rev Cancer.* 2009;9:285–93.
31. Li W, Hu Y, Jiang T, Han Y, Han G, Chen J, et al. Rab27A regulates exosome secretion from lung adenocarcinoma cells A549: involvement of EPI64. *APMIS.* 2014;122:1080–7.
32. Dorayappan KDP, Wanner R, Wallbillich JJ, Saini U, Zingarelli R, Suarez AA, et al. Hypoxia-induced exosomes contribute to a more aggressive and chemoresistant ovarian cancer phenotype: a novel mechanism linking STAT3/Rab proteins. *Oncogene.* 2018;37:3806–21.
33. Meerbrey KL, Hu G, Kessler JD, Roarty K, Li MZ, Fang JE, et al. The pINDUCER lentiviral toolkit for inducible RNA interference in vitro and in vivo. *Proc Natl Acad Sci USA.* 2011;108:3665–70.
34. Ghoshal A, Ghosh SS. Antagonizing canonical Wnt signaling pathway by recombinant human sFRP4 purified from *E. coli* and its implications in cancer therapy. *Mol Cell Biochem.* 2016;418:119–35.
35. Iyer SC, Gopal A, Halagowder D. Myricetin induces apoptosis by inhibiting P21 activated kinase 1 (PAK1) signaling cascade in hepatocellular carcinoma. *Mol Cell Biochem.* 2015;407:223–37.
36. Bosenberg M, Muthusamy V, Curley DP, Wang Z, Hobbs C, Nelson B, et al. Characterization of melanocyte-specific inducible Cre recombinase transgenic mice. *Genesis.* 2006;44:262–7.
37. Oberman F, Rand K, Maizels Y, Rubinstein AM, Yisraeli JK. VICKZ proteins mediate cell migration via their RNA binding activity. *RNA (New Y, NY).* 2007;13:1558–69.
38. Gupta S, Rawat S, Arora V, Kottarath SK, Dinda AK, Vaishnav PK, et al. An improvised one-step sucrose cushion ultracentrifugation method for exosome isolation from culture supernatants of mesenchymal stem cells. *Stem Cell Res Ther.* 2018;9:180.
39. Jao CY, Salic A. Exploring RNA transcription and turnover in vivo by using click chemistry. *Proc Natl Acad Sci USA.* 2008;105:15779–84.